Segmentation of the Surrounding Arteries and Pancreatic Ductal Adenocarcinoma (PDAC) Utilizing A Deep Learning-Based Cascade Method for Pancreatic Tumour Segmentation

Dr. P. Gomathi

Professor, Department of Electronics and Communication Engineering, Study World College of Engineering, Coimbatore, Tamilnadu, India. Email: p.gomathi2006@gmail.com

ABSTRACT

This study proposes a convolutional neural network (CNN)-based approach to segment PDAC mass and nearby arteries in CT images by combining powerful conventional characteristics. TAU-Net is demonstrated by incorporating dense Scale-Invariant Feature Transform (SIFT) & LBP descriptors into the attention U-Net. A 3D-CNN & an ensemble model is then employed to combine the advantages of both networks. Since the sample size was insufficient for vascular segmentation, the previously stated pre-trained networks were used and improved. The recommended method performs 7.52% better than the most advanced DSC methods in PDAC mass segmentation within the portal-venous phase, according to experimental results. Additionally, assessing the response to PDAC treatment can be made easier with the use of three-dimensional visualisation of the tumour and surrounding veins.

Keywords: Artificial intelligence, Endoscopic ultrasound, microbubble, contrast-enhanced and pancreatic cancer.

1. INTRODUCTION

According to some reports, they are also relatively good in diagnosing cancer [1]. These cross-sectional imaging studies may, however, have false-positive outcomes. For example, several studies have demonstrated that when pancreatic tumours were surgically removed, imaging tests revealed malignancies, but the results were negative for neoplastic illness [2]. The correct differential diagnosis of pancreatic tumours so typically requires histological investigation. For the extraction of pathological material from pancreatic tumours, endoscopy ultrasound-guided fine-needles aspiration (EUS-FNA) is crucial because of its high diagnostic yields for malignancy [3,4,5,6]. Although EUS-FNA is thought to be a safe technique, there is still a chance that it could produce false-negative results and that it could cause unfavourable effects including bleeding or pancreatitis from the needle puncture [7].

In addition, needle tract seeding has been shown in individuals treated for pancreatic cancer using EUS-FNA [8,9]. A more precise imaging study without a needle puncture should ideally be used to make the diagnosis. Endoscopic ultrasonography (EUS) is a type of imaging that uses a specialised endoscope Having a high-frequency transducer on the end to make images of the upper intestine with great spatial resolution for the evaluation of pancreatic lesions [10]. Diagnostic accuracy has been significantly improved recently by advancements in a number of image augmented EUS approaches [11,12].

A registration-free deep learning approach was shown by Gibson et al. to segment eight organs, including the pancreatic. In their approach, Roth et al. used a pre-segmented pancreatic framework, a refinement convolutional network, and a holistically-nested network to further improve it. AG modules were suggested by them in order to concurrently highlight relevant regions with significant traits and suppress the irrelevant regions. Using the NIH pancreatic dataset, Man Y et al. segmented the pancreas using a Deep Q Networks (DQN) driven approach with deformable U-Net, and they obtained a state-of-the-art average DSC of 86.93 ± 4.92%. On two datasets, Zhu et al. suggested a progressive 3D coarse-to-fine segmentation method utilising the ResNet bypass structure: the JHMI diseased pancreatic dataset and the NIH pancreas dataset. A convolutional network model was developed by Zhou et al. in another investigation to detect and separate the pancreatic cyst. A summary of our primary contributions is as follows:

- To tackle the challenge of pancreatic tumour segmentation, we suggest a new cascaded automatic neural approach. The two steps of this technique are jointly optimised during training using gradient backpropagation.
- Obtaining more complex feature visualisations of pancreatic tumours is based on multi-scale U-Net. To mitigate the issues of under-segmentation & false positives, we meticulously crafted a focus module and a non-local localisation module to collect target detail feature representations in the second stage.
- We do comparison experiments using various cutting-edge methods with the pancreatic tumour

recognition and pancreas segmentation datasets using the Specificity, sensitivity, and Sørensen–Dice coefficient. According to the trial results, our system performs the best in terms of both visual effects and segmentation assessment indicators.

2. Proposed Methodology

The red highlighted region, which makes up a tiny percentage of the input image, is the pancreatic tumour area, as seen in Figure 1A. This causes erroneous tumor localisation during training since the network is readily perplexed by complicated and fluctuating background information. (2). The green contour line in Figure 1B denotes the pancreatic tumor's perimeter. False positives & under segmentation problems arise throughout the pancreatic tumor segmentation procedure because the tumor has poor contrast with an unclear border line and the surrounding landscape. In order to precisely identify and quantify pancreatic tumors using medical pictures, clinical physicians typically first identify the pancreas' location in order to estimate the range of a tumour. The range is then meticulously identified and narrowed until a distinct pancreatic tumour is found. We suggest a two-stage Segmenting pancreatic tumours using a cascaded automated neural system that is modelled after the physician's diagnostic procedure and gradually segments tumour targets.

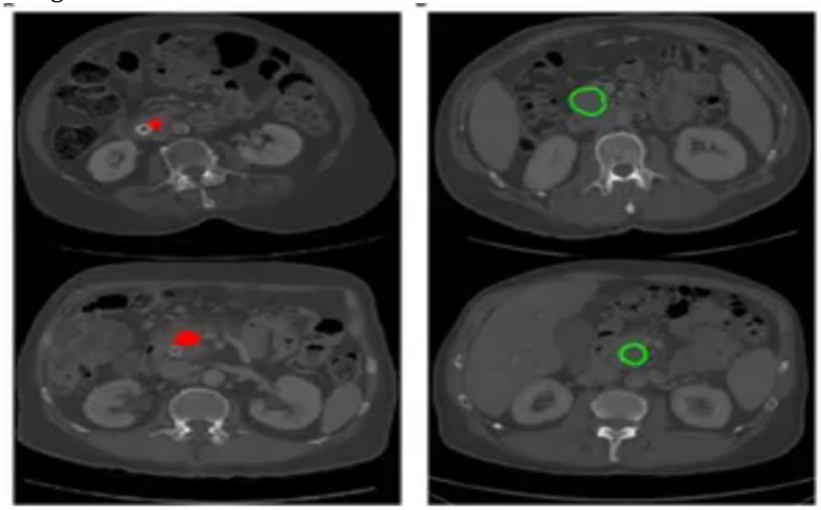

(a) (b)

Figure 1. Distinct labelling schemes for tumours of the pancreas. (A) Labelling the tumour region; (B) Labelling the tumour contour.

Treatment options for locally advanced and borderline resectable PDAC include chemotherapy and radiation therapy. Before beginning any chemoradiation treatment, the tumour volume must be manually assessed, which can be a time-consuming process and intricate process based on the radiologist's background. Artificial volumetric segmentation of important tumours is essential for monitoring and diagnosis. It is crucial to recognise lesions in organs such as the liver, brain, and breast when segmenting medical images. The most often utilised technique for evaluating pancreatic cancer is CT. One of the most difficult tumour segmentation tasks is undoubtedly fully-automated PDAC segmentation in CT scans. The primary challenges in automated tumour and pancreatic segmentation stem from three factors: (1) The pancreas's size, shape, and location, particularly the PDAC mass, might vary, as seen in Fig. 2. (2) The tumour and pancreas are small throughout the CT scan; (3) the contrast is low at the edges.

The two main kinds of organ segmentation techniques are top-down and bottom-up approaches. Top-down approaches use pre-existing knowledge, like atlases or shape models, which are created and integrated into the framework by image registration or shape model fitting. Bottom-up methods employ local picture similarity grouping or labelling based on pixels or voxels. When segmenting problematic organs, the bottom-up approaches work better.The model's sensitivity to target pixels is increased without the need for complex heuristics. While noisy and irrelevant replies are disambiguated, significant aspects are highlighted using a gating module. These steps are taken to fuse the pertinent features right before each skip connection. Equation (1) provides the AG module with both low-level & high-level feature maps.

$$\varphi_{AG} = f_{\varphi}(x) = \text{Sigmoid}(W^{T}.\text{ReLU}(x_1 \oplus x_h)) \quad (1)$$

The linear transformation is shown by W^{T} , the low-level and high-level feature maps are represented by x_l and $x_h$respectively, the attention coefficient is $\text{Sigmoid}(x) = 1/(1 + e^{-x})$, and the matrix addition is indicated by $\oplus$. A low-level feature map is multiplied element-wise by attention coefficients to produce attention features [Eq. (2)].

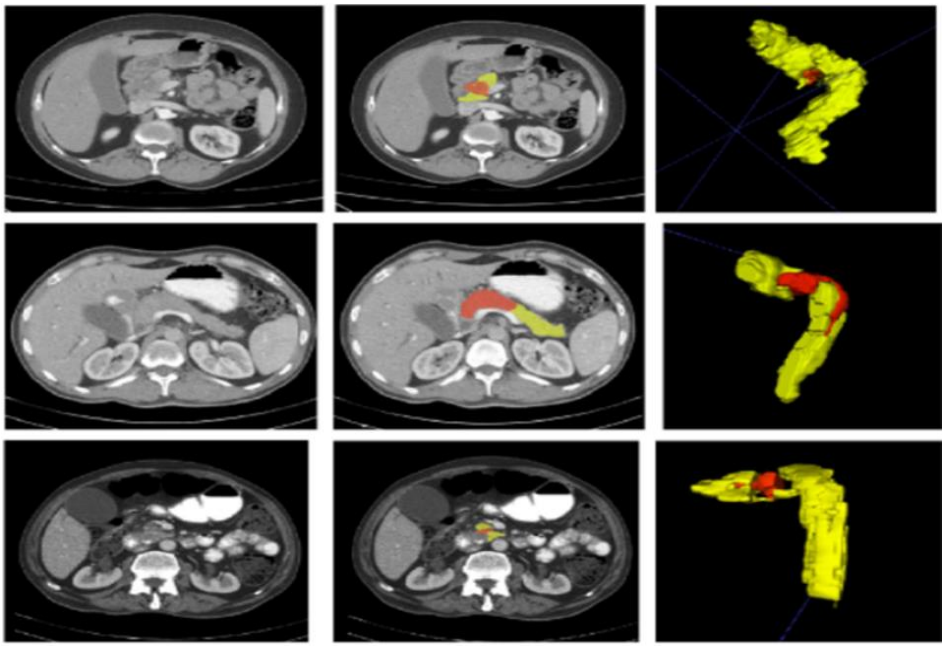

Raw Image Ground truth 3D display

Figure 2. Pancreatic abnormalities, demonstrating the wide range of PDAC mass locations, sizes, and shapes. DAC mass is shown as red, whereas the normal pancreatic region is shown as yellow.

$$\hat{x}_l = \varphi_{AG} \odot x_l \quad (2)$$

where $\odot$ stands for element-wise product, $\varphi_{AG}$is the higher-level features' attention coefficient, and the attention feature is denoted by $\hat{x}_l$.

The output $(x_{h_{new}})$ of this stage is one of the inputs of the gate module. The inputs of the attention gate consist of combined low-level feature maps $x_l$from the coding stage and newly generated high-level feature maps $(x_{h_{new}})$ [Eq. (3)].

$$\hat{x}_l = \left[\text{Sigmoid}\left(W^T.\text{ReLU}\left(W_x^T x_1 + W_x^T x_{h_{new}}\right)\right)\right] x_1 \quad (3)$$

$$x_{h_{new}} = \text{Concat}(x_h, \text{TXFea}) \quad (4)$$

$$\hat{x}_h = U(\text{concat}(\hat{x}_l, x_h)) \quad (5)$$

$\hat{x}_l$in in this case represents attention features, $\hat{x}_h$_hand up-sampling by U represents input to the next step of the decoder route, and$x_{h_{new}}$ represents high-level features combined with texture features.

3. METHODS

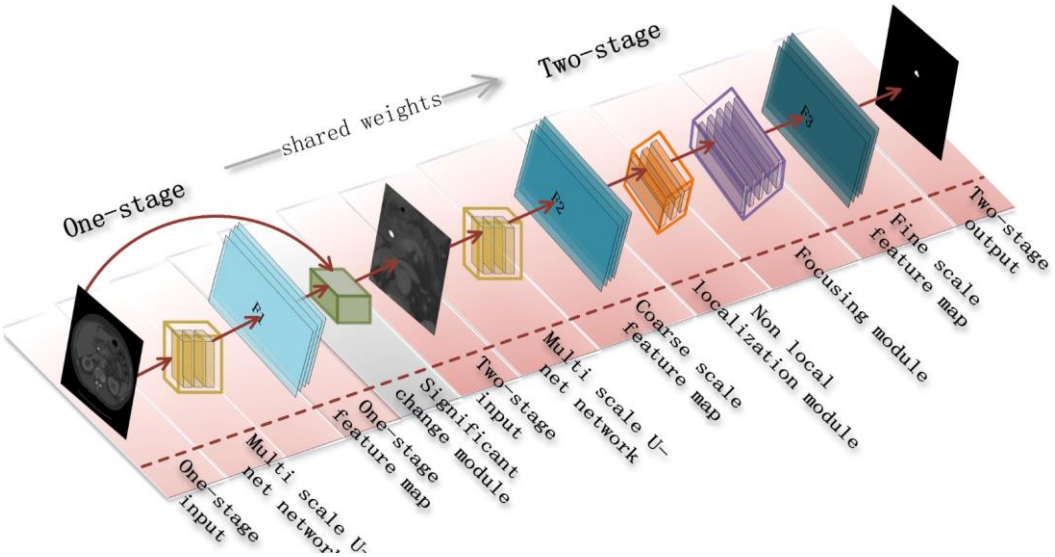

Figure 3. A two-phase approach for pancreatic tumour cascade segmentation.

Accurately identifying pancreatic tumours from an abdominal CT scan is our aim. For pancreatic tumour segmentation, we develop a cascade segmentation neural approach, as shown in Figure 3. The algorithm's two stages depend on a multi-scale U-Net. In the second stage, we meticulously construct a multi-scale U-Net structure

based on concentrating modules and non-local localisation to segment pancreatic tumours, minimising the issues of false positives and under-segmentation. The small-scale pancreatic tumor's minor contribution to the loss function makes it simple to overlook throughout training. We use a common boundary-based metric across classes to help the algorithm generate more robust parameters. The two steps and the loss function settings are then explained in detail.

Weighted cross entropy for pixels (WPCE)

The definition of WPCE loss is as follows:

$$\text{Loss } 1 = \text{WPCE} = -W_c \times U \times \log(V) \quad (6)$$

where the ground truth is U and the expected binary mask is V. nc, $W_c = \frac{nB}{n_c}$ the ratio of the total number of background pixels n_B to the total number of pixels in each class (tumour or pancreas), was chosen as the sample weight for each class in this investigation.

Generalized dice loss (GDL)

Multiple class segmentation has been evaluated using the Generalised Dice Score (GDS), which assigns a single score. A proposed loss function for deep neural network training with extremely imbalanced data is Generalise Dice Loss (GDL):

$$\text{Loss } 2 = \text{GDL} = 1 - 2\frac{\sum_{c=1}^{2} W_c \sum_{i=1}^{N}(V)_{iC} + \varepsilon}{\sum_{c=1}^{2} W_c \sum_{I=1}^{2}(V)_{ic} + (U)_{ic} + \varepsilon} \quad (7)$$

where $W_c = 1/\left(\sum_{i=1}^{N}(U)_{ic}\right)^2$ is a weight is used to offset the effect of different region sizes on data loss, c represents the target class, & ε is used to avoid division by zero.

5. RESULTS

Additionally, Fig. 4 displays the qualitative segmentation results for several CT slices. Findings for two samples of the self-collected dataset appear in rows 3 and 4, whereas two samples of the MSD dataset are displayed in rows 1 and 2. The results' 3D reconstruction using ITK-SNAP (Fig. 4d) displays a realistic and anatomical view with very few imperfections.

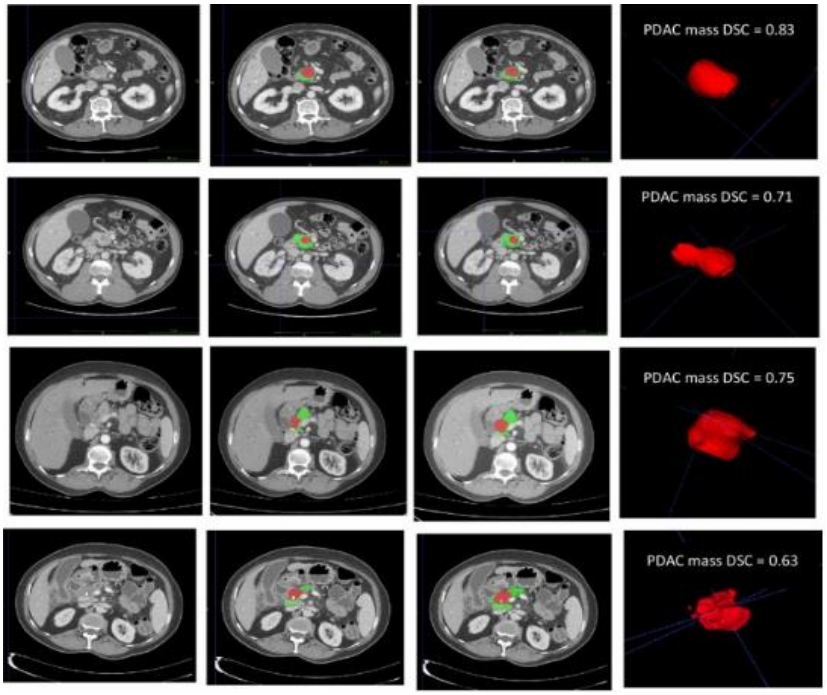

Figure 4. The hybrid network was used to segment the pancreatic and PDAC mass. (a) Initial picture; (b) Ground truth (normal pancreatic tissue is shown in green, and PDAC mass is indicated in red); (c) Completed segmentation; and (d) PDAC mass visualisation in three dimensions.

Combining SIFT, 2D-LBP, and 3D-LBP slices into the selected network layers was investigated in order to integrate texture information. According to experimental results, 3D-LBP outperforms 2D-LBP, as predicted. Figure 5 contrasts a single slice's 2D-LBP with 3D-LBP. Compared to the 2D LBP and the original image, a 2D slice of a 3D-LBP provides much more information.

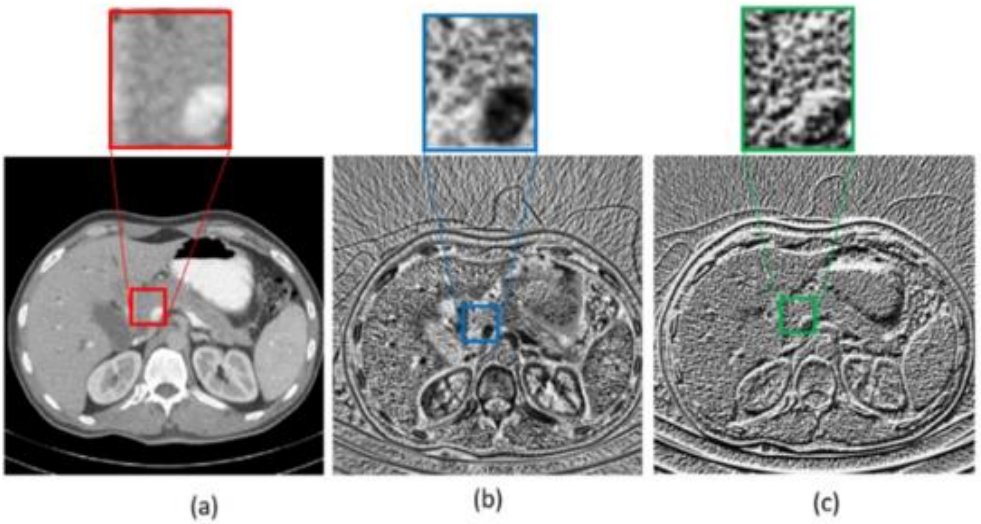

Figure 5. A slice of the original volume is shown in (a), followed by the LBP slice made from the original volume's 3D LBP and the 2D LBP made from the original image.

SIFT maps were added to the network as well. Different step sizes are used to create the SIFT maps, which are then concatenated into the appropriate layer in the decoding route. As a result, during decoding, both high-level and low-level SIFT features benefit from each other. The examination's findings are presented in Table 1, which clearly shows that the duodenal segmentation task is difficult as well as that the dice values from earlier approaches are reasonably close. The two-stage segmentation method is generally more effective than the one-stage method. Our system receives an NIH score of 87.63% for Dice. The performance outperforms the top two-stage segmentation approach, RTUNet, by 1.38% and the best one-stage segmentation method, LMNS-Net, by 2.26%. In terms of SEN & SPE, our system also outperforms earlier segmentation techniques.

Table 1. comparison with the NIH dataset and the most sophisticated pancreatic segmentation methods.

Method	Dice	SEN	SPE
Nishio et .al [24]	0.7890	0.6783	0.9877
Li et al [25]	0.8203	0.7107	0.9865
LMNS –Net [26]	0.8337	0.8015	0.9878
Fixed –point [27]	0.8157	0.6194	0.9868
RSTN [28]	0.8308	0.8366	0.9887
Ours	0.8763	0.9126	0.9988

6. CONCLUSION:

In order to help physicians diagnose pancreatic tumours and in order to facilitate radiation therapy, we have created a two-phase automatic segmentation method. The first step segments the pancreas using a multi-scale network, while the second stage uses the segmentation results to decrease the input area. The first stage's segmentation risk map is used to determine the prior knowledge for the second step. The creation of a multi-scale network with an emphasis on pancreatic tumour segmentation and non-local localisation occurs in the second step. Using class-to-class shared boundary measurements, we create a loss function to address the issue of small-scale targets' inadequate contribution. Our approach outperforms other cutting-edge segmentation techniques on pancreas tumour segmentation exercises, according to many trials. Our technique has a special reference significance in microscopic target segmentation tasks in several sectors, in addition to being advantageous to the medical imaging community.

References

1. Bipat S., Phoa S.S.K.S., van Delden O.M., Bossuyt P.M.M., Gouma D.J., Lameris J.S., Stoker J. Ultrasonography, computed tomography and magnetic resonance imaging for diagnosis and determining resectability of pancreatic adenocarcinoma: A meta-analysis. J. Comput. Assist. Tomogr. 2005;29:438–445.
2. Abraham S.C., Wilentz R.E., Yeo C.J., Sohn T.A., Cameron J.L., Boitnott J.K., Hruban R.H. Pancreaticoduodenectomy (Whipple resections) in patients without malignancy: Are they all 'chronic pancreatitis'? Am. J. Surg. Pathol. 2003;27:110–120. doi: 10.1097/00000478-200301000-00012.
3. Hewitt M.J., McPhail M.J., Possamai L., Dhar A., Vlavianos P., Monahan K.J. EUS-guided FNA for diagnosis of solid pancreatic neoplasms: A meta-analysis. Gastrointest. Endosc. 2012;75:319–331. doi: 10.1016/j.gie.2011.08.049.
4. Yoshinaga S., Itoi T., Yamao K., Yasuda I., Irisawa A., Imaoka H., Tsuchiya T., Doi S., Yamabe A., Murakami Y., et al. Safety and efficacy of endoscopic ultrasound-guided fine needle aspiration for pancreatic masses: A prospective multicenter study. Dig. Endosc. 2020;32:114–126. doi: 10.1111/den.13457.

5. Tanaka K., Hayashi T., Utsunomiya R., Takigawa Y., Kobayashi Y., Nagai K., Kin T., Yane K., Takahashi K., Shinohara T., et al. Endoscopic ultrasound-guided fine needle aspiration for diagnosing pancreatic mass in patients with surgically altered upper gastrointestinal anatomy. Dig. Endosc. 2020;32:967–973. doi: 10.1111/den.13625.
6. Kurita Y., Kuwahara T., Hara K., Mizuno N., Okuno N., Matsumoto S., Obata M., Koda H., Tajika M., Shimizu Y., et al. Features of chronic pancreatitis by endoscopic ultrasound influence the diagnostic accuracy of endoscopic ultrasound-guided fine-needle aspiration of small pancreatic lesions. Dig. Endosc. 2020;32:399–408. doi: 10.1111/den.13497.
7. Kanno A., Yasuda I., Irisawa A., Hara K., Ashida R., Iwashita T., Takenaka M., Katanuma A., Takikawa T., Kubota K., et al. Adverse events of Endoscopic Ultrasound-Guided Fine-Needle Aspiration for Histologic Diagnosis in Japanese Tertiary Centers: A Multicenter Retrospective Study. Dig. Endosc. 2020 doi: 10.1111/den.13912.
8. Yane K., Kuwatani M., Yoshida M., Goto T., Matsumoto R., Ihara H., Okuda T., Taya Y., Ehira N., Kudo T., et al. Non-Negligible Rate of Needle Tract Seeding after Endoscopic Ultrasound-Guided Fine Needle Aspiration for Patients Undergoing Distal Pancreatectomy for Pancreatic Cancer. Dig. Endosc. Off. J. Japan Gastroenterol. Endosc. Soc. 2020;32:801–811. doi: 10.1111/den.13615.
9. Hatamaru K., Kitano M. Can early diagnosis of EUS-FNA needle tract seeding for pancreatic cancer improve patient prognosis? Dig. Endosc. 2020;32:742–744. doi: 10.1111/den.13719.
10. Iwashita T., Uemura S., Mita N., Iwasa Y., Ichikawa H., Senjyu A., Yasuda I., Shimizu M. Utility of endoscopic ultrasound and endoscopic ultrasound-guided fine-needle aspiration for the diagnosis and management of pancreatic cystic lesions: Differences between the guidelines. Dig. Endosc. 2020;32:251–262. doi: 10.1111/den.13579.
11. Crino S.F., Brandolese A., Vieceli F., Paiella S., Conti Bellocchi M.C., Manfrin E., Bernardoni L., Sina S., D'Onofrio M., Marchegiani G., et al. Endoscopic Ultrasound Features Associated with Malignancy and Aggressiveness of Nonhypovascular Solid Pancreatic Lesions: Results from a Prospective Observational Study. Ultraschall Med. 2021;42:167–177. doi: 10.1055/a-1014-2766.
12. Banerjee, J. et al. (eds) 3D LBP-Based Rotationally Invariant Region Description Asian Conference on Computer Vision (Springer, 2012). Simpson, A. L. et al. A large annotated medical image dataset for the development and evaluation of segmentation algorithms. http://arxiv.org/abs/190209063 (2019).
13. Yushkevich, P. A. et al. User-guided 3D active contour segmentation of anatomical structures: Significantly improved efficiency and reliability. Neuroimage **31**(3), 1116–1128 (2006).
14. Lowe, D. G. Distinctive image features from scale-invariant keypoints. Int. J. Comput. Vision **60**(2), 91–110 (2004).
15. Ojala, T., Pietikainen, M. & Maenpaa, T. Multiresolution gray-scale and rotation invariant texture classification with local binary patterns. IEEE Trans. Pattern Anal. Mach. Intell. **24**(7), 971–987 (2002).
16. Ioffe, S. & Szegedy, C, editors. Batch normalization: Accelerating deep network training by reducing internal covariate shift. International Conference on Machine Learning (2015).
17. Tokunaga, H., Teramoto, Y., Yoshizawa, A. & Bise, R, editors. Adaptive weighting multi-field-of-view CNN for semantic segmentation in pathology. Proceedings of the IEEE/CVF Conference on Computer Vision and Pattern Recognition (2019).
18. Pasyar, P. et al. Hybrid classification of diffuse liver diseases in ultrasound images using deep convolutional neural networks. Inform. Med. Unlocked. **22**, 100496 (2021).
19. Buda, M., Maki, A. & Mazurowski, M. A. A systematic study of the class imbalance problem in convolutional neural networks. Neural Netw. **106**, 249–259 (2018).
20. Sudre, C. H., Li, W., Vercauteren, T., Ourselin, S. & Cardoso, M. J. Generalised Dice Overlap as a Deep Learning Loss Function for Highly Unbalanced Segmentations. Deep Learning in Medical Image Analysis and Multimodal Learning for Clinical Decision Support 240–248 (Springer, 2017).
21. Bokhovkin, A. & Burnaev, E. (eds) Boundary Loss for Remote Sensing Imagery Semantic Segmentation. International Symposium on Neural Networks (Springer, 2019).
22. Csurka, G., Larlus, D., Perronnin, F. & Meylan, F. editors. What is a good evaluation measure for semantic segmentation? BMVC (2013).
23. 50. Nishio M, Noguchi S, Fujimoto K. Automatic pancreas segmentation using coarse-scaled 2d model of deep learning: usefulness of data augmentation and deep u-net. Appl Sci. (2020) 10:3360. doi: 10.3390/app10103360
24. Li M, Lian F, Wang C, Guo S. Accurate pancreas segmentation using multi-level pyramidal pooling residual u-net with adversarial mechanism. BMC Med Imaging. (2021) 21:1–8. doi: 10.1186/s12880-021-00694-1.
25. Paithane P, Kakarwal S. Lmns-net: Lightweight multiscale novel semantic-net deep learning approach used for automatic pancreas image segmentation in ct scan images. Expert Syst Appl. (2023) 234:121064. doi: 10.1016/j.eswa.2023.121064.
26. Zhou Y, Xie L, Shen W, Wang Y, Fishman EK, Yuille AL. (2017). A fixed-point model for pancreas segmentation in abdominal ct scans, in: International conference on medical image computing and

computer-assisted intervention, . pp. 693–701. Springer-Verlag Berlinheidelberger Platz 3, D-14197 Berlin, Germany: Springer.

27. Xie L, Yu Q, Zhou Y, Wang Y, Fishman EK, Yuille AL. Recurrent saliency transformation network for tiny target segmentation in abdominal ct scans. IEEE Trans Med Imaging. (2019) 39:514–25. doi: 10.1109/TMI.42